Received: 9 September 2016 | Revised: 17 May 2017 | Accepted: 8 September 2017

DOI: 10.1111/exsy.12245

WILEY Expert Systems

ARTICLE

An inference model for combustion diagnostics in an experimental oil furnace

A.T. Fleury | F.C. Trigo | A.L. Pacífico | F.P.R. Martins

Escola Politecnica - Mechanical Engineering Department, Universidade de Sao Paulo, São Paulo, Brazil

Correspondence
F. C. Trigo, Escola Politecnica - Mechanical Engineering Department, Universidade de Sao Paulo, São Paulo, Brazil.
Email: trigo.flavio@usp.br

Funding information
Conselho Nacional de Desenvolvimento Científico e Tecnológico, Grant/Award Number: 471115/2004-5 and 484260/2011-1

Abstract

The continuous monitoring of the air/fuel ratio, oil/water/air temperatures, and gas/particulate emissions of combustion processes in oil-based furnaces allows experts to detect anomalies and act to prevent faults and critical conditions. These important but tedious tasks can be performed by an expert system designed to mimic the human abilities of recognizing relevant patterns and finding their most likely causes. In this article, we present the architecture of an expert system that uses flame images grabbed during the combustion process in an experimental oil furnace as input parameters. Computational processing of those images provides feature vectors for analysis by "artificial experts" that correlate changes in flame appearance with typical combustion states. The Dempster–Shafer method is used to build the knowledge base and the inference engine. The results of tests in which flame conditions are suddenly modified by altering the physical variables of the combustion process revealed that the method can properly combine measures from various flame image characteristics to issue diagnostics. Such diagnostics are similar to those given by human experts. This suggests that the proposed approach may fill the gap between models based on features extracted from images and real-world operating conditions. This is the intended contribution of this work.

KEYWORDS

combustion diagnosis, furnace monitoring, image analysis, the Dempster–Shafer method

1 | INTRODUCTION

Several industrial processes are monitored by a team of experts that evaluate the flow of input data coming from a large matrix of heterogeneous sensors through a supervisory system equipped with graphical interfaces and auxiliary tools to facilitate the decision-making process. This kind of problem has been a subject in the area of Industrial Information Integration. Chen (2016) conducted a survey over several databases in Web of Science and selected approximately 500 papers on the subject "Industrial Information Integration." Those papers were reviewed and divided into 37 groups, according to research subject, in order to establish the current stage of development and to detect trends and demands for future work in that field.

In typical refining furnaces, sensor failures or incorrect analysis could seriously endanger the plant. For instance, the extinction of a flame can normally be detected by an automatic control loop. However, detection of numerous shortcomings and systemic failure events that degrade furnace performance can only be achieved using the technical knowledge of experts combined with their natural pattern-recognition ability.

To optimize the capacity of a furnace, it is necessary that it work under the supervision of a robust control system. Nevertheless, this can only be done if the domain expertise is properly represented and applied. This problem has been thoroughly investigated by several authors, but there are still numerous paths to be explored.

Given the high nonlinearity exhibited by the plant of a stoker-fired boiler, Li and Chang (2000) designed a fuzzy proportional integral derivative system to control the air and the coal flows. With the help of human experts, triangular fuzzy membership functions were synthesized, giving rise to a fuzzy knowledge base from which the fuzzy values of input variables can be inferred. The actions necessary to control the boiler were also represented in this fuzzy knowledge base, and after defuzzification, the rules were applied according to the data flow demand.

The article of Cho, Ro, Kim, Jang, and Shon (1998) focused on designing an expert system for a pilot incinerator plant. The knowledge base was composed of a set of crispy "if-then" heuristic rules that represent the expertise of operators. Measures of temperature, pressure, exhaust gases, and solid particulate concentrations are used by an inference engine to supervise the plant, identifying anomalies and proposing corrections.

Chakravarthy, Vohra, and Gill (2000) studied the effect of several operational parameters of an experimental furnace with the goal of designing a software-based sensor to estimate the NO_x emission rate. Thereby, they launched a campaign to collect measures of NO_x emissions according to an experimental matrix encompassing variations in fuel oil pressure, preheat temperatures and excess air. Finally, a genetic algorithm was applied to estimate the constants of the NO formation dynamical model in order to minimize the difference between the theoretical results and the experimental data.

Using a laboratorial pilot plant, Tronci, Baratty, and Servida (2002) carried out a series of experiments for identifying the concentrations of outlet gases (CO, NO_x, and O_2) according to the type of fuel (pulverized coal, natural gas, and oil) and the values of relevant variables of the process, such as thermal load, excess air, and primary to secondary air flow rates. Those data were used to train and validate a 3-level feedforward artificial neural network that was used as a virtual sensor to estimate the concentration of gases emitted by a furnace.

Hernández & Ballester (2008) adopted a set of averaged flame images captured on a gas-based experimental furnace. These images were the only data source used to identify different combustion states encompassing parameterized variations on the primary-to-secondary air ratio and on the swirl numbers of both the streams. The NO_x emissions were measured for all those states, and feature vectors composed of geometric and luminosity parameters were calculated for the corresponding images. Then, a Kohonen artificial neural network was trained to classify the images according to the self-similarity degree of their feature vectors. As showed by the authors, the trained neural network was able to correctly classify image flames not originally present in the training set but did not exhibit a good performance concerning the estimation of NO_x emissions.

Sequences of images of flames grabbed on an experimental furnace were also used by Fleury, Trigo, and Martins (2013) as the only source for identifying changes in atomization quality, a characteristic of oil-based combustion processes strongly affected by the steam-to-fuel rate. They constructed a training set composed of flame image feature vectors associated with *a priori* known steam-to-fuel rates and used a fuzzy rule to classify those vectors according to their respective flame atomization quality. Then, the combined use of a Kalman filter and a random-walk model permitted them to successfully estimate atomization quality for new flames. In further work, Silva, Fleury, Martins, and Ponge-Ferreira (2015) investigated flames stability, another relevant aspect of furnace operation. The researchers used operational modal analysis techniques to estimate a 4-degree-of-freedom second-order model of flame dynamics. Training sets of feature vectors obtained from flame images corresponding to known primary-to-secondary air flows (and consequently, known levels of stability) provided the data necessary to build the model.

The ultimate goal of designing models that attempt to predict flame dynamics should be to use those models to establish automatic, less human-dependent control strategies. An attempt to accomplish this task was made by Fleury, Chui, Trigo, and Martins (2015), who incorporated the previous model (Silva *et al*., 2015) in a linear-quadratic controller designed to keep flame stability. However, the connection between a model built upon parameters that are alien to the combustion process and physical quantities that might effectively be used as control inputs, such as the air-fuel rate, was not established.

Considering that a flame exhibits visual characteristics that depend on complex physical phenomena resulting from the assignment of operational parameters, a robust image-based control policy for a furnace cannot be implemented unless the diagnostics issued by the monitoring system is based on a matrix of expert sensors that are able to establish one-to-several cause-and-effect relationships between visual features and combustion states in a similar manner a human being would do. Making robust decisions by combining heterogeneous signals—a typical problem concerning Industrial Information Integration Engineering (Chen, 2016)—is an issue that can be properly approached by inference methods based on belief functions, as reported in the recent literature (Benslama, Batatia, & Messai, 2016; Jamrozik, 2015; Kessentini, Burger, & Paquet, 2015; Pande, Sondawale, Keswani, & Walke, 2015).

In the present article, a new approach aimed at filling the gap between models based on features extracted from flame images and real-world operating conditions is proposed and evaluated. A framework for reasoning under uncertainty based on the Dempster–Shafer method (Basir & Yuan, 2007; Murphy, 1998; Sentz & Ferson, 2002) is adopted. The preliminary results provided by such a framework, that is, the identification of similar visual features in flames generated under distinct operational conditions, indicate that this approach could be useful to construct an extra set of observers for controlling combustion processes in oil refinery furnaces.

2 | EXPERIMENTAL SET-UP AND DATA

All the experiments necessary to generate the data referred to in the present article were carried out on an experimental vertical furnace with 4 m height and 1.5 m internal diameter. On the bottom, a burner equipped with two air ports supplying manually controlled primary and secondary flows (Figure 1) is able to process up to 80 kg/h of heavy fuel oil (87% C, 11% H, 1% S, 1% N: mass base; 620 cSt at 60 °C), and an aperture on the top permits exhaust gases to escape. Water cooled hatches containing the optical devices are located at housing furnace points where the flame can be properly viewed.

Flame images were captured by a monochromatic RS-170 CCD video camera coupled to a 6 mm lens (f/1.2) and to a narrow pass band (±10 nm) interferometric filter at 900 nm reference wave length. The camera output composed video signals, sampled at 25 Hz by a frame grabber, which are transferred to computer memory as a sequence of interlaced 640 × 480-pixel images.

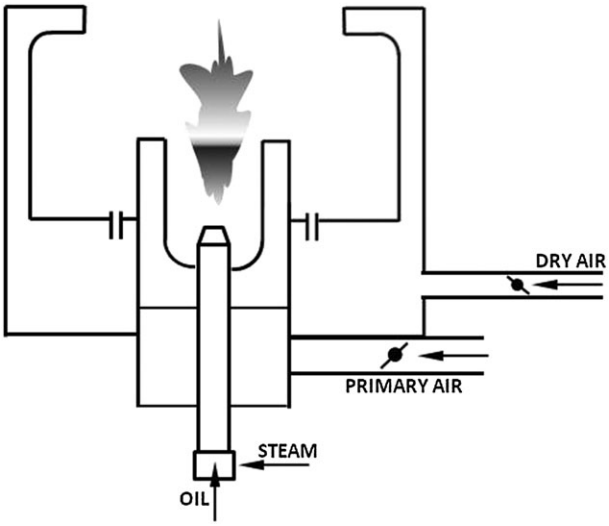

FIGURE 1 Burner schematics (adapted from Fleury et al., 2013)

To implement a design of experiments to investigate the influence of relevant operational variables in the visual aspect of the flames, several additional sensors were properly installed in the furnace, encompassing manometers and pressure transducers, flow rate metres (gear for fuel, differential pressure for air and steam), thermocouples (types T and K), and gas analysers for combustion products (O_2, CO, NO_x, HC, and SO_x).

The campaign to collect experimental data focused on the aspects of the operation that can be investigated by observing the flame's appearance in terms of continuity, stability, symmetry, air excess adequacy, and atomization quality. By properly adjusting the control variables, nine different categories of flames were generated, for which the saliency of a particular feature permitted an expert furnace operator to designate them either as "stable," "unstable," "extinct," "well atomized," "poorly atomized," "normal excess air," "high excess air," "low excess air," or "asymmetric" flames.

Figure 2a–f show images of flames with different degrees of stability. Figure 2a shows the image of a flame generated when the primary-to-secondary air flow rate (*psafr*) was set to 1.0. This image represents a very stable flame. At the other end of the scale, Figure 2f shows the image of a very unstable flame generated when *psafr* = 4.0. It must be emphasized that a crispy classification made by the furnace operator established that the images of Figure 2a–c and 2d–f are members, respectively, of the stable and unstable flames sets.

In Figure 3a–c, a typical process of flame extinguishment can be observed. It is characterized by the sudden appearance of a luminance pattern radiated by the furnace walls, followed by its gradual fading until complete disappearance.

Examples of flames with gradually declining atomization quality can be observed in the sequence of images in Figure 4a–f. The first image shows a flame generated when the steam-to-fuel rate (*sfr*) was set to 0.57, and the last image shows a flame when this parameter was set to 0.17. Higher values of *sfr* contribute to a finer distribution of fuel droplet sizes and a more homogeneous spray (well atomized), which produces flames with high luminance. Low values of *sfr* cause an uneven distribution of droplet sizes and larger sizes of droplets (poorly atomized), generating less luminance of the flame and a coarser texture of the captured images (Lefebvre, 1989). According to the crispy classification used by the expert operator, images 4a–c represent well atomized flames, whereas the remaining images 4d–f represent poorly atomized ones.

Images of Figure 5a–h are examples of flames exhibiting different excess air ratios (*ea*). The expert classified the first two images (Figure 5a–b) as normal excess air flames, the following three images (Figure 5c–e) as high excess air flames, and the remaining images (Figure 5f–h) as low excess air flames. Noteworthy is the fact that moderate-low excess air (1% to 2%) contributes to a higher formation of soot. This fine particulate material irradiates around the visible yellow and orange colours, contributing to a more luminescent image of the flame, as can be seen in Figure 5f–g. For excess air values below 1%, the lack of oxygen and the unburned fuel mitigates the luminance of the flame, as shown in Figure 5h (Turns, 2012).

In Figure 6a–b, it is possible to appreciate the difference between a geometrically normal flame, generated when the fuel flows through all the six spray nozzle outputs, and an asymmetric one, which is the product of partially obstructed nozzle outputs.

Table 1 presents the values of furnace operational parameters required to generate the flame images belonging to the nine categories referred to in the previous paragraphs.

It is important to emphasize that although the images of Figures 2–6 correspond to flames generated under different furnace operational conditions, they naturally share several common visual characteristics. As a consequence, it is not an easy task, even for an experienced operator, to identify the correct condition of an operational furnace through the observation of a single flame.

The images of Figures 2a and 5g, for instance, are not so distinct, despite the first and second being the result of the setting *ea* = 3.0 (normal excess air) and *ea* = 1.0 (low excess air), respectively, and all the remaining parameters are maintained at their reference values (see Table 1). Moreover, the noticeable geometrical asymmetry exhibited by both images of Figures 4a and 6b could lead someone to conclude that nozzle outputs were partially obstructed at the time both flames were generated. That inference is correct for the second image (Figure 6b), but not

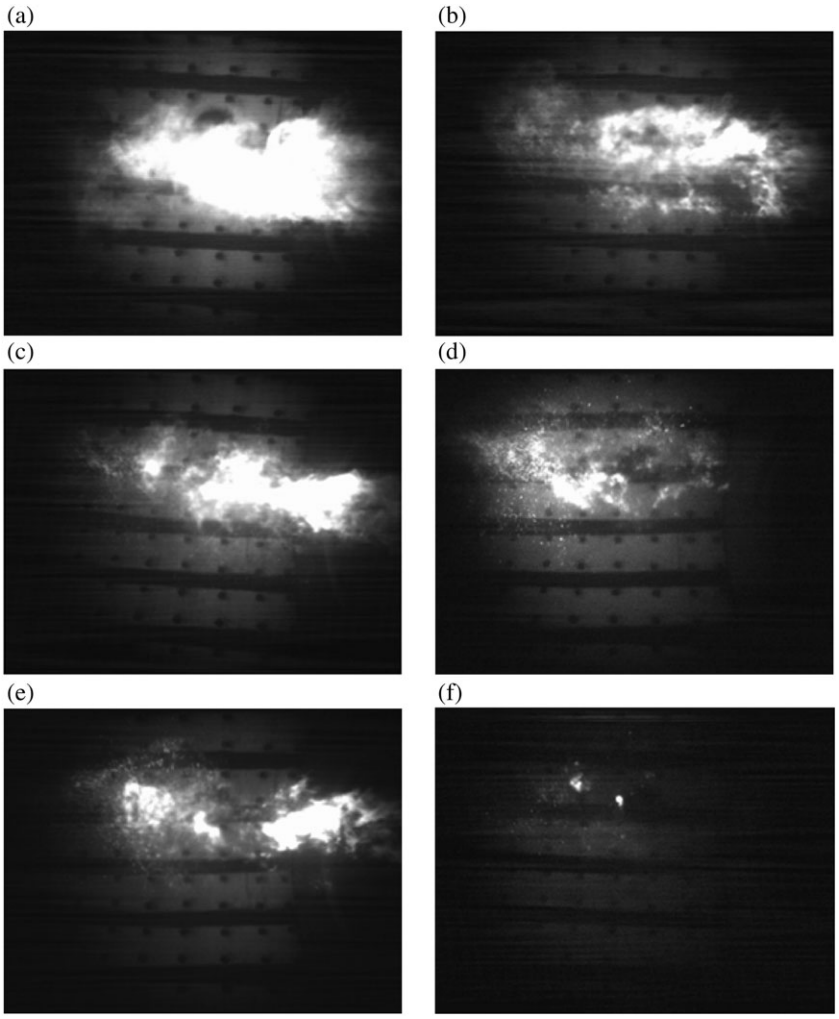

FIGURE 2 Flames generated for different primary to secondary air flows: (a) *psafr* = 1 × 1; (b) *psafr* = 1.5 × 1; (c) *psafr* = 1.9 × 1; (d) *psafr* = 2.3 × 1; (e) *psafr* = 3 × 1; (f) *psafr* = 4 × 1

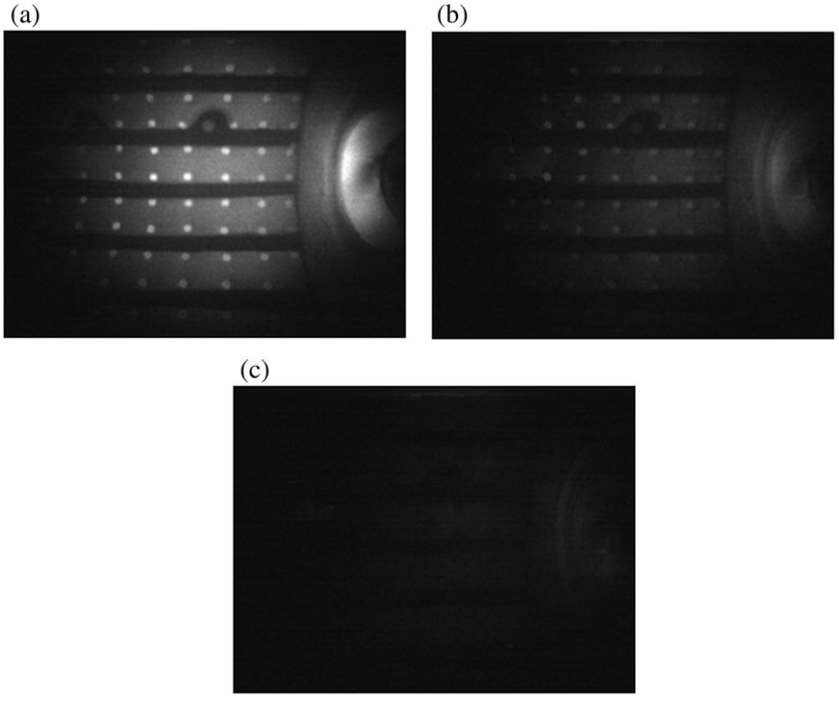

FIGURE 3 Flame extinction sequence

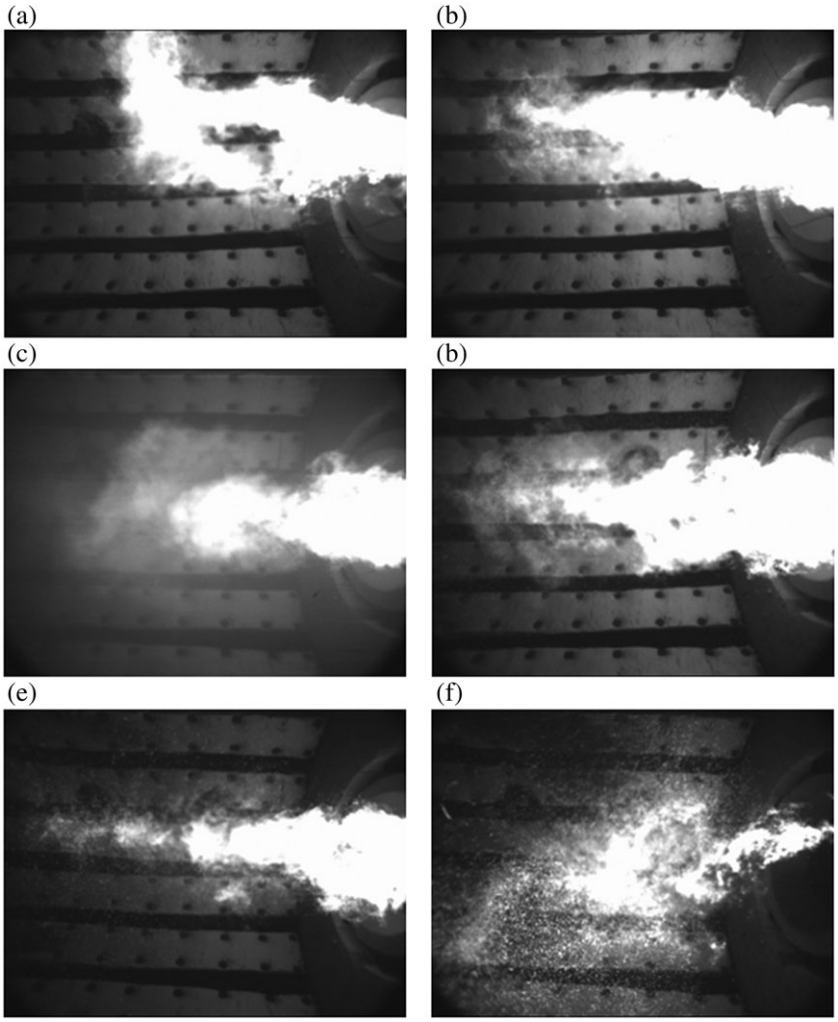

FIGURE 4 Flames generated for different steam to fuel rates: (a) *sfr* = 0.57; (b) *sfr* = 0.43; (c) *sfr* = 0.29; (d) *sfr* = 0.23; (e) *sfr* = 0.21; (f) *sfr* = 0.17

for the first (Figure 4a). Several other erroneous inferences could result if only few characteristics of the images were considered. For instance, if the classification were based only on two features, "average grey level" and "degree of uniformity," the images of Figures 2f (unstable flame), 3b–c (extinct flame), and 5h (low excess air) could receive the same classification.

3 | IMAGE FEATURE VECTORS

A large spectrum of image-based classification problems (Malamas, Petrakis, Zervakis, Petit, & Legat, 2003; Pandit & Bhiwani, 2015; Ranjidha, Kumar, & Saranya, 2013) are usually approached through the abstraction of highly spatially correlated images (like the ones considered in this article) into vectors of distinctive visual features. Such a practice permits to eliminate redundancy, improve reliability, and reduce the classification algorithm's training time. In the domain of combustion diagnosis, flame images are usually subsumed by vectors whose components are related to geometric, luminance, and texture features (Hernández & Ballester, 2008; Santos-Victor, Costeira, Tomé, & Sentieiro, 1993; Yan, Lu, & Colechin, 2002).

For the problem focused on in this article, a set of 33 image features related to shape geometry, grey-level distribution, texture, and spatial frequency composition were selected to create a knowledge base representing human expertise to identify a likely furnace operational state when a given combination of distinctive visual features is observed in the flame.

Concerning the original flame images (like the ones in Figures 2–6) and their grey level histograms and co-occurrence matrices (Gonzalez & Woods, 2008; see Figure 7), the following image properties are calculated as follows:

f_1 = average grey level;

f_2 = image information entropy, given by

$$f_2 = -\sum_{i=1}^{255} p(j)\ln_2(j), \tag{1}$$

where $p(j)$ represents the frequency of occurrence of grey level j in the image;

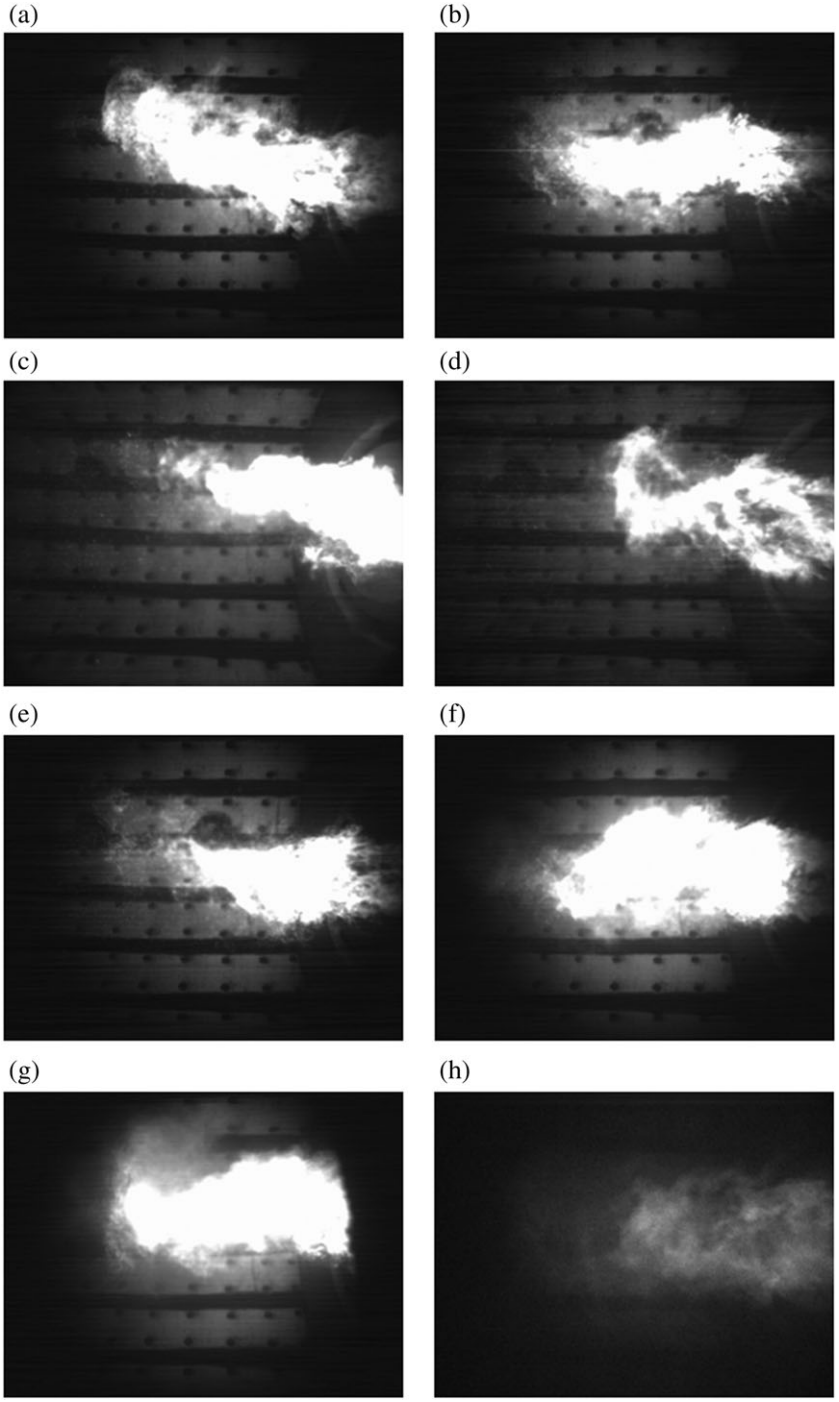

FIGURE 5 Effect of the excess air (*ea*) in the flames appearance: (a) *ea* = 3.8%; (b) *ea* = 3.0%; (c) *ea* = 8%; (d) *ea* = 7%; (e) *ea* = 5%; (f) *ea* = 1.5%; (g) *ea* = 1.0%; (h) *ea* = 0.6%

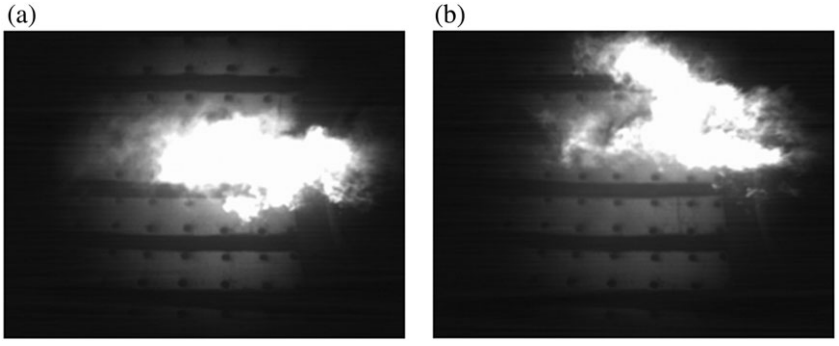

FIGURE 6 (a) Symmetric flame; (b) Asymmetric flame

TABLE 1 Experimental matrix operational parameters

Category	Fuel flow	Primary air flow secondary air flow (psafr)	Excess air (%; ea)	Steam to fuel rate (sfr; mass base)	Obstructed nozzle outputs
Stable	Permanent	1.00, 1.50, 1.86	3.0	0.33	None
Unstable	Permanent	2.33, 3.00, 4.00	3.0 < ea < 3.8	>0.33	None
Extinct	Interrupted	1.00	3.0	0.33	None
Well atomized	Permanent	1.00	3.0 < ea < 3.8	0.57, 0.50, 0.43, 0.36, 0.29	None
Poorly atomized	Permanent	1.00	3.0 < ea < 3.8	0.26, 0.23, 0.21, 0.17	None
Normal excess air	Permanent	1.00	3.0, 3.8	0.33	None
High excess air	Permanent	1.00	5.0, 6.0, 7.0, 8.0	0.33	None
Low excess air	Permanent	1.00	0.6, 1.0, 1.5	0.33	None
Asymmetric	Permanent	1.00	3.0 < ea < 3.8	0.33	Two out of six

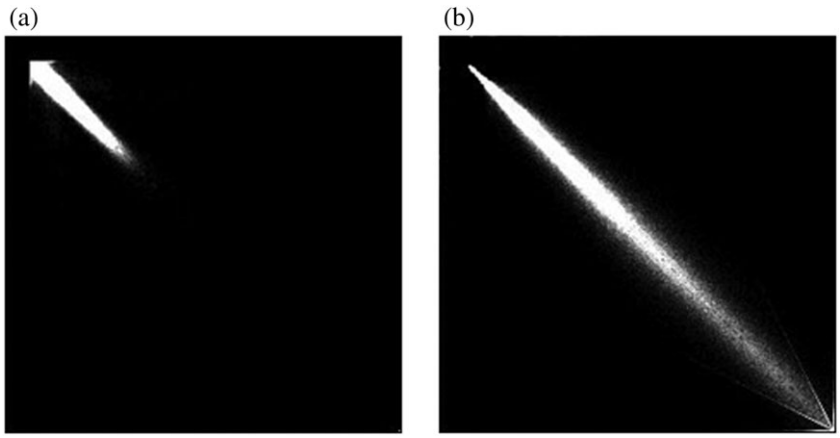

FIGURE 7 Co-occurrence matrix images based on a horizontal neighbourhood of size 1: (a) From image of Figure 2f; (b) From image of Figure 4f

f_3 = co-occurrence matrix energy, given by

$$f_3 = \sum_{i,j}[c(i,j)]^2; \tag{2}$$

f_4 = co-occurrence matrix contrast index, given by

$$f_4 = \sum_{i,j}|i-j|^2 c(i,j); \tag{3}$$

f_5 = co-occurrence matrix homogeneity index, given by

$$f_5 = \sum_{i,j}\frac{c(i,j)}{1+|i-j|} \tag{4}$$

(in Equations 2–4, $c(i,j)$ is the normalized value of the co-occurrence matrix at line i, column j);

f_6 to f_{18}: grey level frequencies of occurrence taken on 13 equally spaced intervals of the grey level histogram of the image.

After applying the 2D Fourier transform to the original flame images (see examples shown at Figure 8a–c) and obtaining their respective co-occurrence matrices, three additional texture characteristics, f_{19} (co-occurrence matrix energy), f_{20} (contrast index), and f_{21} (homogeneity index), are extracted from those matrices.

Flame binary images, generated after applying Otsu's method (Otsu, 1979) to the original grey level ones, and their respective contours, (see Figure 9a–b), give rise to 12 more features, as follows: f_{22}–f_{23}: x and y sizes of the image circumscribed rectangle; f_{24}: image area; f_{25}–f_{26}: x and y coordinates of the image centroid; f_{27}–f_{28}: x and y second-order moments of the image; f_{29}: image perimeter; f_{30}–f_{31}: x and y coordinates of the image contour centroid; f_{32}–f_{33}: x and y second-order moments of the image contour.

Properties f_1, f_2, and f_6 to f_{18} summarize the image's luminance distribution; properties f_1, f_2, f_3, and f_{19}, f_{20}, and f_{21} subsume the textural spatial characteristics of the image and of its power spectrum, respectively; and finally, properties f_{20} to f_{32} describe the main geometric characteristics of the flames. Changes of one or several of the operational variables *psafr*, *ea*, or *sfr* impaired the temperature distribution, and consequently affected the image luminance, geometry, texture, and spatial frequency composition. Likewise, obstruction of one or more nozzles gives rise to sharp changes in flame geometry. All those effects and causes (changes to *psafr*, *ea*, *sfr*, and the degree of obstruction of the nozzle outputs) are linked

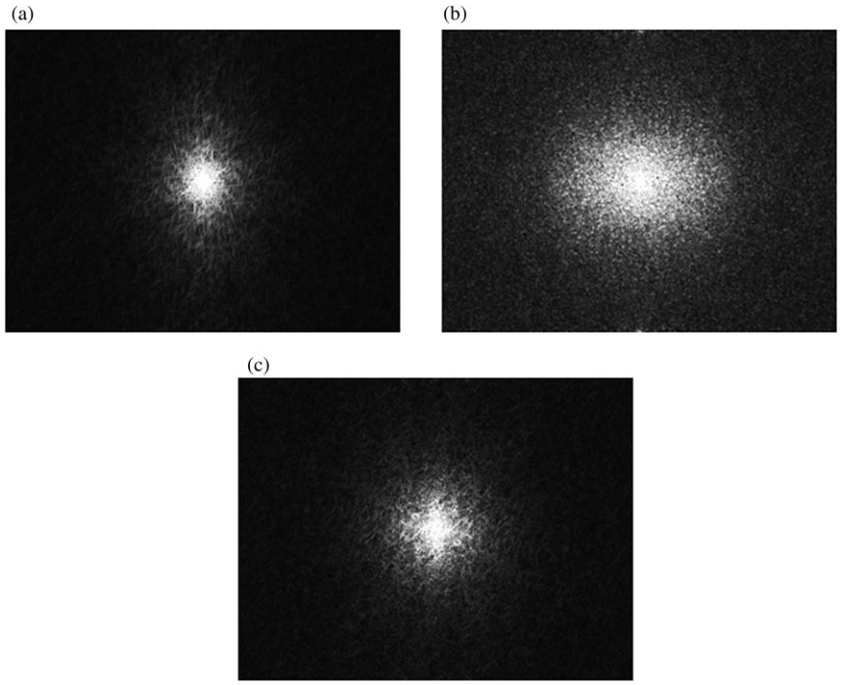

FIGURE 8 Magnitude of the 2D Fourier transform of images shown at: (a) Figure 1a; (b) Figure 3f; (c) Figure 5e

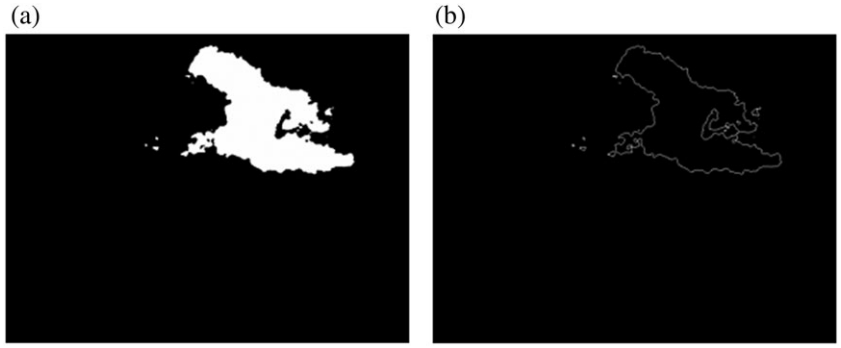

FIGURE 9 (a) Thresholded image of Figure 6 b; (b) Its respective contour

in a nontrivial way. Thus, we need to construct an inference engine to generate classification criteria from flame images that have been previously classified by a human expert.

Using suitable functions available in Matlab®, the feature vectors described above were calculated for all the flame images grabbed during the experimental campaign. It is important to observe that those images are automatically classified into one of the nine categories mentioned before because they are linked to a previously designed experimental matrix. Those classified feature vectors contain the basic elements to be used in an inference process aimed at identifying furnace combustion states.

Partitioning of these feature vectors sets, on a two-to-one basis, gives rise to a training set and a test set. The former is used to build the system knowledge base, the subject of the next session. The latter is used to validate the inference method, as will be discussed in Section 6.

4 | KNOWLEDGE REPRESENTATION

The Dempster–Shafer knowledge base has to provide previously defined assumptions encompassing all possible *OR* combinations (hereafter, the symbol ∨ will be used where necessary) of n diagnostics taking values on a set Θ, which is named the *frame of discernment*.

For the problem focused in this article, $n = 9$ and Θ is represented by

$$\Theta = \{1, 2, 3, 4, 5, 6, 7, 8\}, \tag{5}$$

where the indices 1 to 9 correspond to the categories stable, unstable, extinct, well atomized, poorly atomized, normal excess air, high excess air, low excess air, and asymmetric, respectively.

Considering that $2^9 = 512$ combined *OR* diagnostics α ($\alpha \in 2^{\Theta}$, where 2^{Θ} is the set of all subsets of $\Theta - \Phi$, and Φ= empty set) must be taken into account, the training set feature vectors described in the previous section are organized as follows.

Nine singleton sets $F_{\{1\}}, F_{\{2\}}, \ldots, F_{\{9\}}$ are set-up to contain feature vectors of flames from categories $1, 2, \ldots, 9$, respectively. Thirty six $\left(36 = C_2^9\right)$ double-folded *OR* (represented by the character ∨) sets $F_{\{1,2\}}, F_{\{1,3\}}, \ldots, F_{\{1,9\}}, F_{\{2,3\}}, F_{\{2,4\}}, \ldots, F_{\{2,9\}}, \ldots, F_{\{8,9\}}$ are also created to contain the feature vectors of flames from both categories $1 \vee 2, 1 \vee 3, \ldots, 1 \vee 9, 2 \vee 3, 2 \vee 4, \ldots, 2 \vee 9, \ldots, 8 \vee 9$, respectively.

Eighty-four tripleton *OR* sets, 126 4-folded *OR* sets, and so on are organized accordingly to the same rule indicated before. Finally, one 9-folded *OR* set $F_{\alpha = \{1,2,3,4,5,6,7,8,9\}}$ is arranged to contain the feature vectors of all flames, that is, $1 \vee 2 \vee 3 \vee 4 \vee 5 \vee 6 \vee 7 \vee 8 \vee 9$.

After the 512 feature vectors sets *F_α*have been assembled, they are submitted to a knowledge synthesis process that subsumes all the occurrences of their components $f_i^\alpha = 1, \ldots, 33$ by the corresponding pairs of parameters $\left(u_i^\alpha, \sigma_i^\alpha\right)$ that represent the best-fitted Gaussian distribution to f_i^α. Such a process produces 512 synthesized files S_α, each one containing 33 rules associating the subset α of *OR combined* individual diagnostics taken in Θ with the parameters of a normal distribution. A partial view of one of these files is presented in Table 2.

Hence, the system knowledge base is composed by all those 512 files S_α, each one storing 33 s_i^α independent assertions such as that implicitly stated at the second column (s_2) of file $S_{\{1,4,6,8\}}$: "The probability distribution of the information entropy of the images of flames analysed up to now and belonging to categories stable or well atomized or normal excess air or low excess air, is Gaussian with $\mu = 6.49$ and $\sigma = 0.25$."

However, from the Dempster–Shafer framework point of view, a rule such as the one enunciated above must be interpreted as a piece of *a priori* knowledge of a member of a group of experts that investigate a problem of their domain of knowledge. Thus, extending the previous example, it can be said that "expert" s_2 knows how to calculate the entropy of information of flame images and how to use such a measure to attribute probabilities for 512 events concerning classification of the flame in every one of the subsets of 2^Θ. In other words, the knowledge of expert s_2 s_2 is represented by 512 assertions such as the one stated above, and the same occurs with the other 32 experts.

5 | DEMPSTER–SHAFER INFERENCE ENGINE

Figure 10 illustrates the main steps required to make inferences on flame images and issue diagnostics about the combustion process according to the basic framework of the Dempster–Shafer method.

Following the block diagram of Figure 10, a new flame image $I(t)$, grabbed at instant t, is submitted to preprocessing, which produces a 33-component feature vector

$s(t) = (s_1(t), s_2(t), \ldots, s_{33}(t))$ and is then dispatched to a set of elementary knowledge bases $KB_i, i = 1, \ldots, 33$.

Every KB_i takes the component $s_i(t)$ of $\overrightarrow{s}(t)$ and calculates 512 values m_α^i ($\alpha \in 2^\Theta$), named "attributed probabilities" (Sentz & Ferson, 2002), according to

$$m_\alpha^i = \exp\left(-\frac{1}{2}\left(\frac{s_i(t) - \mu_\alpha^i}{\sigma_\alpha^i}\right)\right). \tag{6}$$

Such values are not true probabilities; instead, they should be interpreted as the degree of membership of the flame to the subset α of *OR* combinations one up to nine diagnostics of Θ.

Then, a function implementing the Dempster–Shafer combination rule is applied in a recursive way. Hence, the original 512 so-called "worlds" W^1 (Hughes & Cresswell, 1972) generated by KB_1 and characterized by the sets $\alpha \in 2^\Theta$ and their respective probabilities m_α^1 are combined with the worlds W^2 generated by KB_2, according to

$$m_{W^{1^2}}^{1^2} = \frac{1}{1-K} \sum_{W^1, W^2 : W^1 \cap W^2 = W^{1^2}} m_{W^1}^1 . m_{W^2}^2, \tag{7}$$

where

$$K = \sum_{W^1, W^2 : W^1 \cap W^2 = \Phi} m_{W^1}^1 . m_{W^2}^2 \tag{8}$$

is a measure of the degree of contradiction between evidence provided by the worlds W^1 and W^2. In the above formulae, the symbol ∧ stands for "and."

TABLE 2 Partial view of file $S_{\{1,4,6,8\}}$

	s_1	s_2	s_3	s_4	...	s_{32}	s_{31}	s_{32}	s_{33}
μ	79.95	6.49	0.3430	0.0341	...	398	274	3.50E + 06	1.61E + 07
σ	14.75	0.25	0.0658	0.0059	...	43	20	1.99E + 06	7.24E + 06

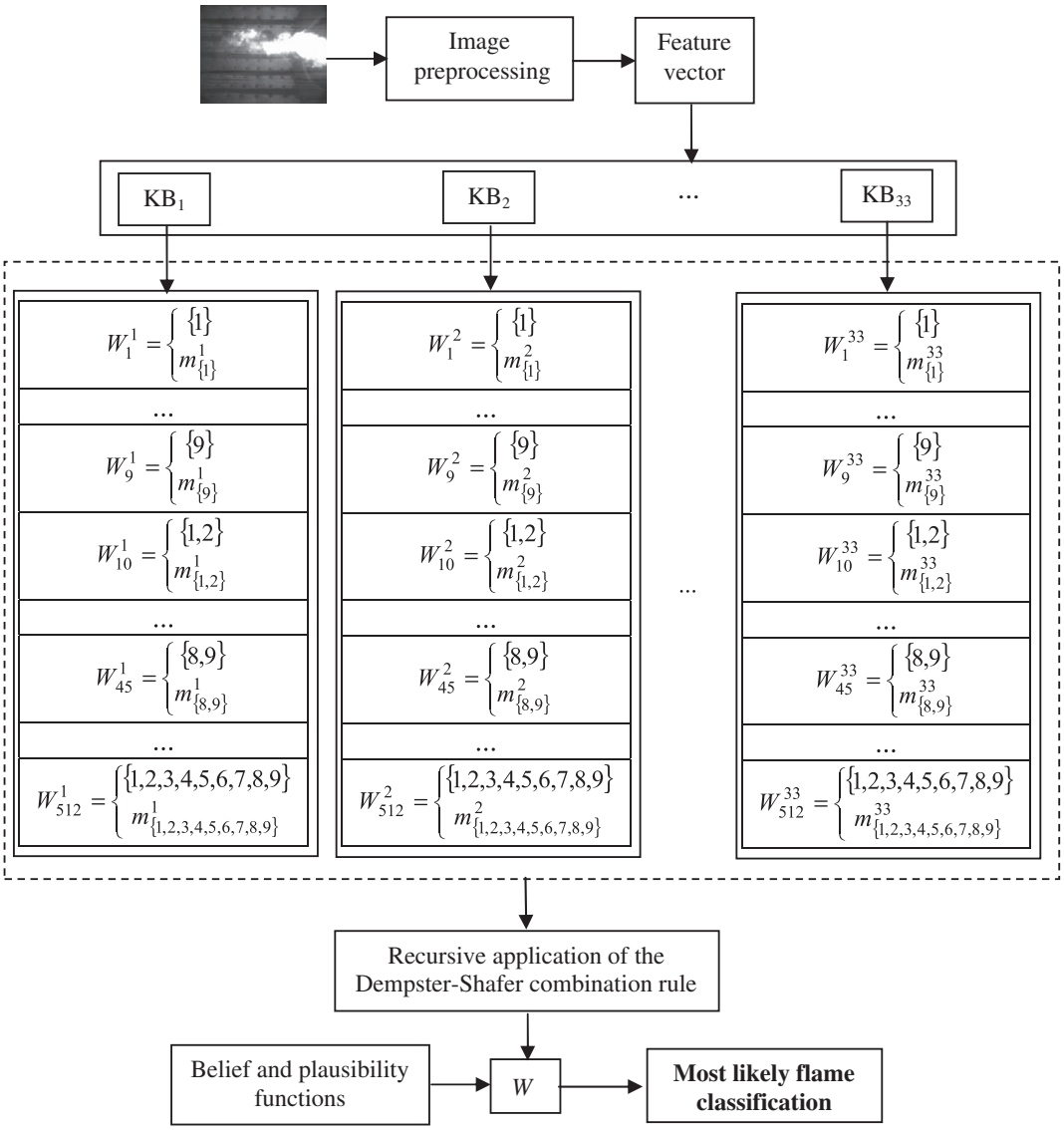

FIGURE 10 Dempster–Shafer inference engine for flame image classification

This first step of the application of the Dempster–Shafer combination rule gives rise to new $N_1 \leq 512$ worlds $W^{1\wedge 2}$. A second application of the same rule, combining all instances of $W^{1\wedge 2}$ and W^3, gives rise to new $N_2 \leq 512$ worlds $W_i^{(1^2)^3}$. This process of data fusion continues until all the worlds generated by the 33 experts are combined altogether in a set of $N_{33} \leq 512$ final worlds W.

As a last step of the algorithm, the "degree of belief" and the "degree of plausibility" of every diagnostic $D_i \in 2^{\Theta}$, are calculated, respectively, by the functions

$$Bel(D_i) = \sum_{W_i : W_i \subseteq D_i} m_{Wi} \tag{9}$$

$$Pl(D_i) = \sum_{W_i : W_i \cap D_i = \Phi} m_{Wi} \tag{10}$$

that are named *belief* and *plausibility* functions. It is important to emphasize that the probability $P(D_i)$ that diagnostic D_i is correct satisfies the relation

$$Bel(D_i) \leq P(D_i) \leq Pl(D_i) \ldots$$

Therefore, the m_{Di} (the attributed probability to D_i and the interval $[Bel(D_i), Pl(D_i)]$) can be used to estimate the likelihood that image $I(t)$ exhibits visual characteristics of flames belonging to the set D_i.

6 | RESULTS

Matlab® was the basis to implement a prototype computer system for reading and processing streaming images, calculating their feature vectors, consulting knowledge bases, combining worlds W and their respective attributed probabilities, m, and finally calculating the corresponding belief and plausibility functions according to the paradigm of the Dempster–Shafer method.

To ascertain that the Dempster–Shafer algorithms were correctly implemented and that such a method was suitable to approach the focused problem, a series of verification tests based on the analysis of the plausibility of the diagnostics were performed. The well-known drawback of the Dempster–Shafer rule, which concerns combinations of high-conflicting worlds (Zadeh, 1986), was properly dealt with. A heuristic rule is always applied before making the combination of two worlds, and if the degree of inconsistency between them is higher than a maximum threshold value K_{max}, the process is bypassed. Aiming at reducing the demanding processing time, after each fusion cycle, a heuristic rule drops from memory all the worlds whose attributed probabilities are lower than a minimum predefined threshold value, m_{max}.

The temporal process data flow presented in Figure 10 was applied for several sequences of test images belonging to two or three distinct categories of flames. Hence, in all those sequences, a sudden transition between the values of the combustion parameters occurs at a given moment, causing the visual appearance of flames to abruptly change.

In Table 3, a summary of the tests performed so far is presented. The second column lists the sequences of transitions from first to last of each test, whereas the third and fourth columns give the intervals containing image frames with the same characteristics. As the test set images were grabbed at a 25 Hz frequency, the time interval between instants i and $i + 1$equals 1/25 s. It must also be noted that the reason why the sequences shown encompass different numbers of images is that some tests, such as the ones focusing on asymmetry and atomization quality, exhibited a rich variety of diagnostics across time, whereas the others behaved much more uniformly.

Figures 11, 12 show plots of belief and plausibility functions of Test 1 for nine singleton subsets of 2^{θ}. It should be mentioned that computations for the remaining 503 subsets are actually performed but not drawn because they do not have major significance for the diagnostic. This reduction is essential for the curves to be discernible. The same simplification is applied to similar graphs of the other three tests.

Correct interpretation of the results exhibited by the above referred plots demands the analysis of the belief and plausibility functions. Considering instant $i = 0$, for example, with a focus on the most likely diagnostic, "1" (stable),

$$Bel(0) = 0.65$$

meaning that 0.65 is the total support given to the proposition "At instant $i = 0$, the flame is stable" by the evidence arising from the remaining worlds of 2^{θ}containing multifold diagnostics. In other words, it can be said that the above proposition is true with 0.65 confidence.

On the other hand,

$$Pl(0) = 0.69$$

meaning that there is $1 - 0.69 = 0.31$ evidence that At instant $i = 0$, the flame is stable is a false statement. According to the Dempster–Shafer paradigm, the remaining "probability mass," representing the gap between the supporting and the disproving evidence concerning the given proposition, that is, $1 - 0.65 - 0.31 = 0.04$, is the uncertainty level of the inference.

Therefore, it could be finally said that the composed proposition

"*At instant* $i = 0$, the *flame is stable* is true with 0.65 confidence ∧

At instant $i = 0$, the *flame is stable* is false with 0.31 confidence"

has an uncertainty level of 0.04.

TABLE 3 List of tests performed

Test	Flame characteristics	First instant (frame i)	Last instant (frame i)
1	Stable Unstable Extinct	0 10 21	9 20 30
2	With normal excess air With high excess air With low excess air	0 10 23	9 22 37
3	Well atomized Badly atomized	0 26	25 36
4	With normal excess air Asymmetric	0 26	25 66

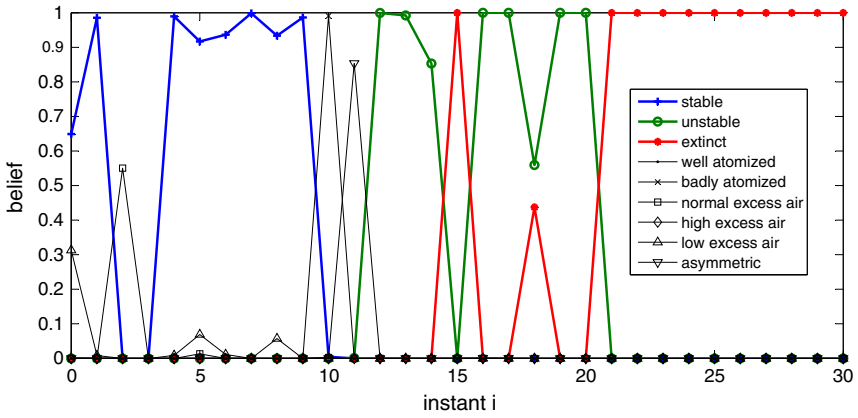

FIGURE 11 Belief functions for Test 1: Transition from stable to unstable to extinct

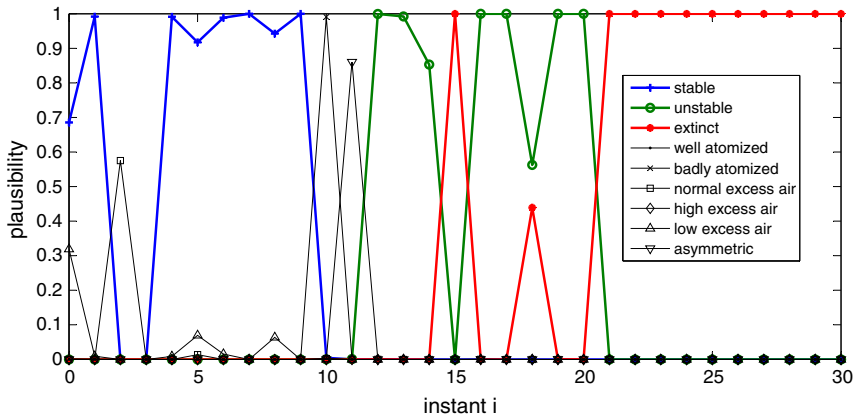

FIGURE 12 Plausibility functions for Test 1: Transition from stable to unstable to extinct

By repeating this analysis for all the nine singleton diagnostics shown in the graphs and if necessary, for the most likely remaining multifold diagnostics of 2^{θ}, a comprehensive diagnostic picture can be issued at every instant. In those plots, the coloured curves correspond to the nominal diagnostics of Test 1. The same agreement is adopted for the respective plots from Tests 2–5.

To simplify the analysis, the graph of Figure 13 exhibits the most likely diagnostic issued by the method across time based on the highest values of the belief functions of the worlds of 2^{θ}.

In Figure 13, ordinate values higher than nine represent multifold diagnostics. For instance, at the instant $i = 3$, when the method issues the ambiguous diagnostic $8 \vee 1$, meaning that the appearance of that particular flame had visual characteristics common to either stable or low excess air classes of flames, the ordinate 81 is assigned. Another noticeable fact emerges at instant $i = 2$: a member of the stable flames test set was classified as a normal excess air flame, which is a correct classification, because $ea = 3\%$ (normal excess air) was set-up during the experiments to generate flames exhibiting different levels of stability. The remaining stable flames, up to the instant $i = 9$, received the expected classification 1.

In the subsequent group of unstable flames, four odd diagnostics may be highlighted. At instant $i = 10$, the flame was sorted out as badly atomized—an apparent failure of the method. However, a subjective comparison between the image considered at that instant (Figure 14a) and a typical member of the badly atomized flame images (Figure 14b) indicates that they share some visual features that could give rise to the above cited inference failure.

At instant $i = 11$, the unstable flame (shown in Figure 15) was considered as asymmetric, a diagnostic that cannot be regarded as incorrect, because instability can give rise to flames exhibiting asymmetric shape.

Finally, at instant $i = 15$, the unstable flame was graded as extinct, a misclassification that arises from the fact that, in sequences of very unstable flames, one that almost does not contrast with the background is very likely to appear. The remaining sequence of images belonging to the extinct flames test set was all correctly classified.

In Figures 16–18, the results of Test 2, concerning detection of variation of excess air, are presented. Considering the first 10 image flames, comprising members of the normal excess air test set, the method issued only two ambiguous diagnostics, at instants $i = 5$ ($6 \vee 7$ i.e., normal excess air or high excess air) and $i = 9$ ($6 \vee 8$, i.e., normal excess air or high excess air); the remaining ones were correct and unambiguous.

Diagnostics issued for the next group of images of high excess air flames were correct, except for two inconclusive inferences at instants $i = 15$ ($6 \vee 7$, i.e., normal excess air or high excess air) and $i = 20$ ($8 \vee 7$, i.e., low excess air or high excess air).

For the last sequence of images of low excess air flames, the diagnostics reported by the method were mostly correct. Two ambiguities occur at instants $i = 23$ ($1 \vee 8$) and $i = 31$ ($1 \vee 8$). A plausible, although unexpected, diagnostic occurs at instant $i = 35$, when the flame was classified as

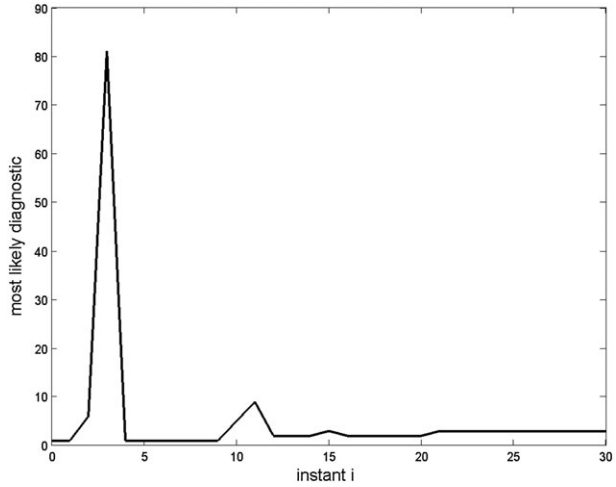

FIGURE 13 Test 1: Most likely diagnostics

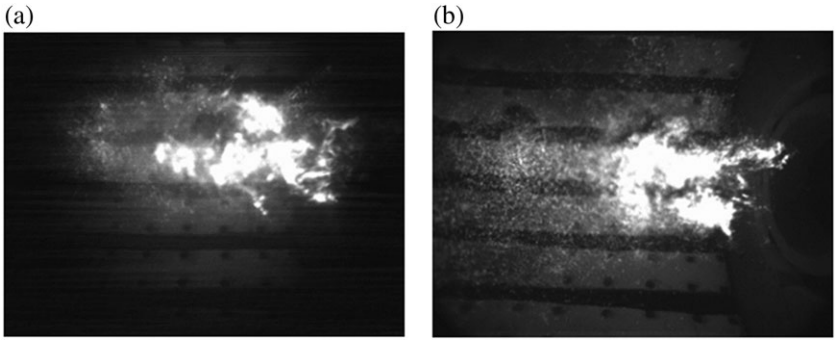

FIGURE 14 Test 1: (a) Unstable flame analysed by the method at instant $i = 10$; (b) A typical badly atomized flame

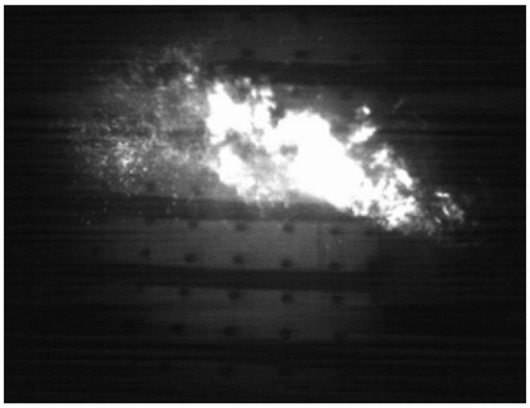

FIGURE 15 Test 1: Asymmetric unstable flame

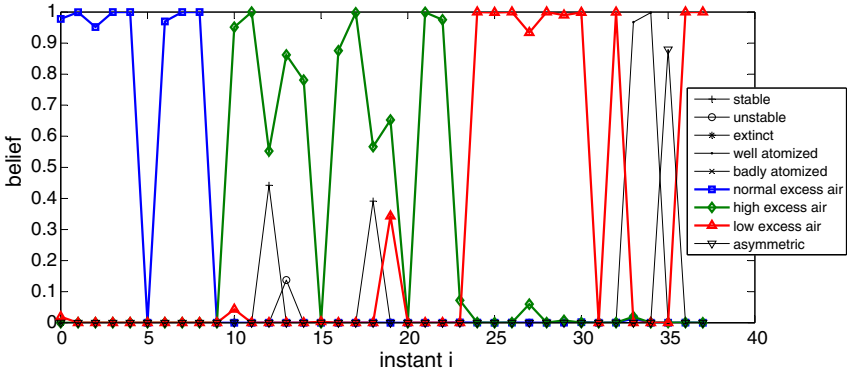

FIGURE 16 Belief functions for Test 2: Transition from normal to high to low excess air

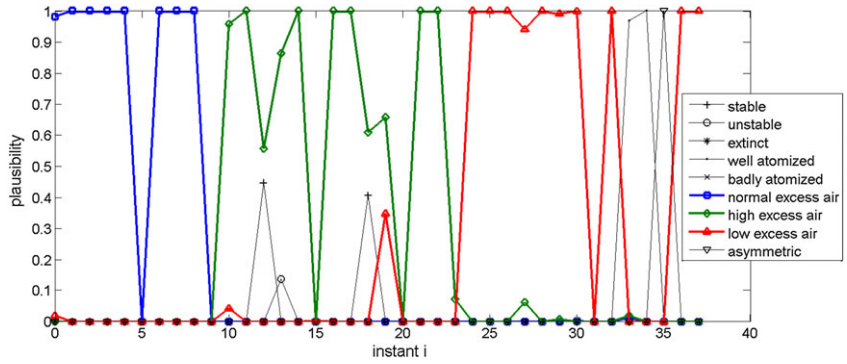

FIGURE 17 Plausibility functions for Test 2: Transition from normal to high to low excess air

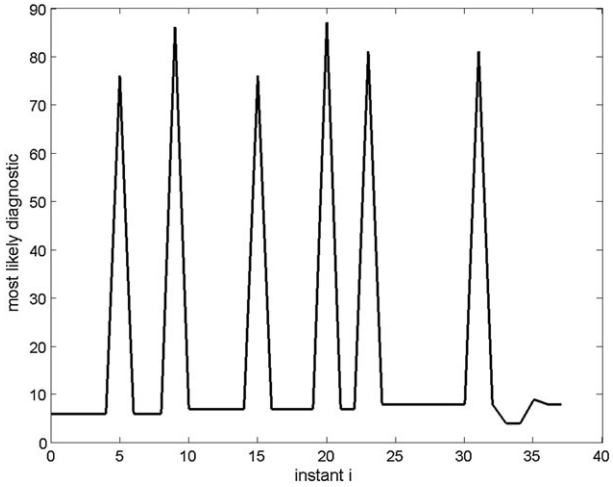

FIGURE 18 Most likely diagnostics for Test 2: Transition from normal to high to low excess air

asymmetric, a decision that could be explained by the very low excess air of the combustion process giving rise to instability and consequently to asymmetry. Two other unexpected diagnostics emerged at instants $i = 33$ and $i = 34$, when the image flames were considered members of the well atomized flames test set. These two last classifications could not be properly explained, so they should be attributed to the lack of feature vector components able to properly distinguish all the visual characteristics of the images.

Figures 19–21 present the results of Test 3, which addresses the discrimination of well atomized flames from the badly atomized ones. Referring to Figure 19, it can be seen that all the diagnostics issued by the method were correct, with the exception of those at $i = 5$ and $i = 7$, when the well atomized flames were classified as low excess air ones. Again, this misbehaviour of the system should be attributed to the same cause discussed in the last paragraph.

Finally, the results for Test 4 are presented in Figures 22–24.

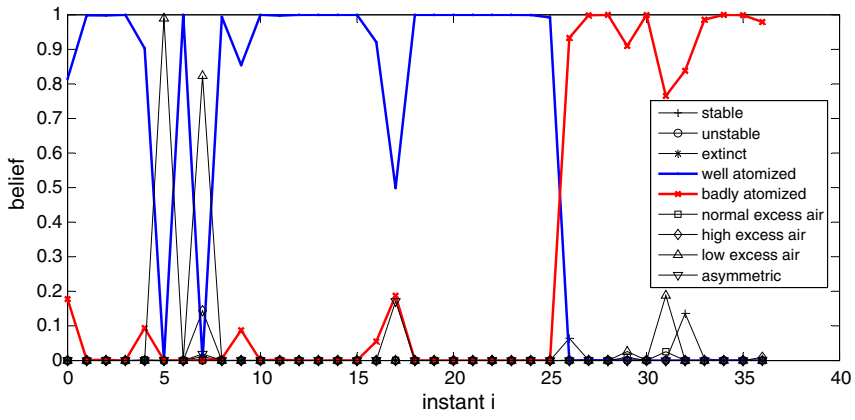

FIGURE 19 Belief functions for Test 3: Transition from well atomized to badly atomized

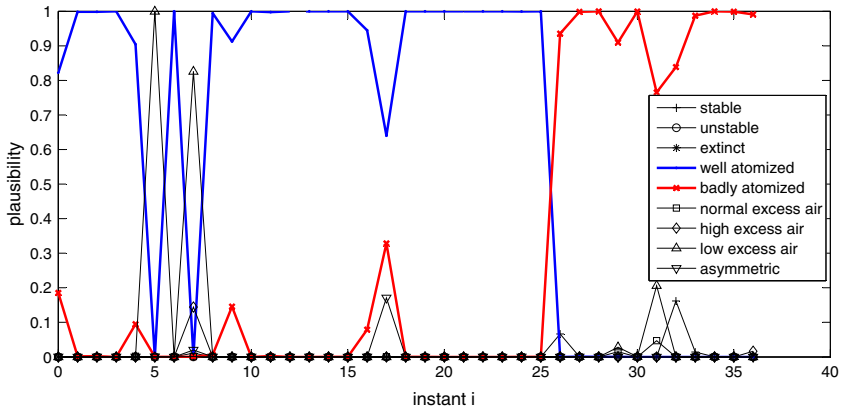

FIGURE 20 Plausibility functions for Test 3: Transition from well atomized to badly atomized

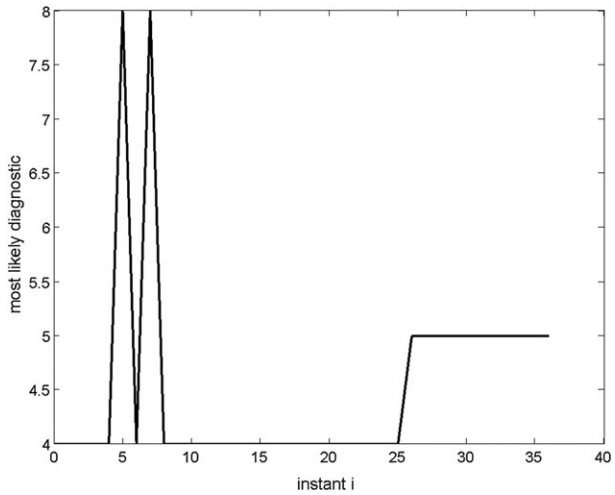

FIGURE 21 Most likely diagnostics for Test 3: Transition from well atomized to badly atomized

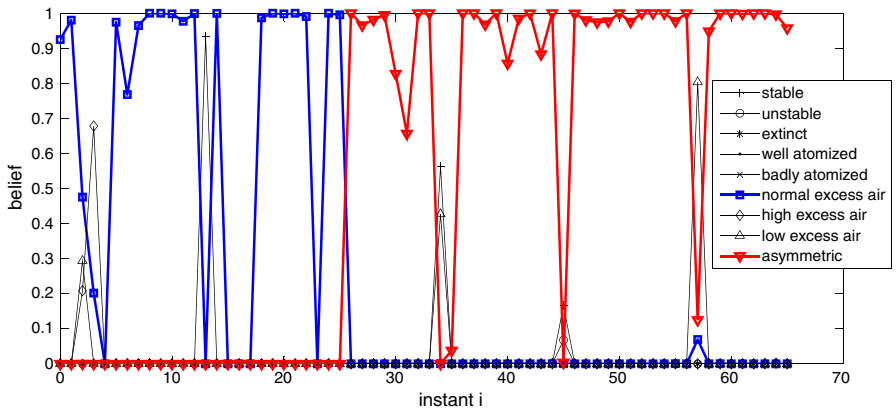

FIGURE 22 Belief functions for Test 4: Transition from normal excess air to asymmetric

The classifications reported by the system for the first sequence of images of normal excess air flames were nearly all correct. A flaw (low excess air) occurred at instant $i = 3$, a plausible diagnostic (stable) was presented at $i = 13$, and five ambiguous classifications were issued at $i = 4$, $i = 15$, $i = 16$, $i = 17$, and $i = 23$, all expressing confusion between classes normal excess air and high excess air.

The majority of the diagnostics issued for the next sequence of images from asymmetric flames set were also correct, despite two inconsistencies: One at $i = 57$, when the flame was classified as low excess air (a failure, because asymmetric flames were generated setting up $ea = 3.0\%$), and other at instant $i = 35$ ($1 \vee 8$), both of which were ambiguous and incorrect. A plausible diagnostic (stable) was presented at $i = 34$, and an ambiguous but plausible ($8 \vee 9$) diagnostic was reported at instant $i = 45$.

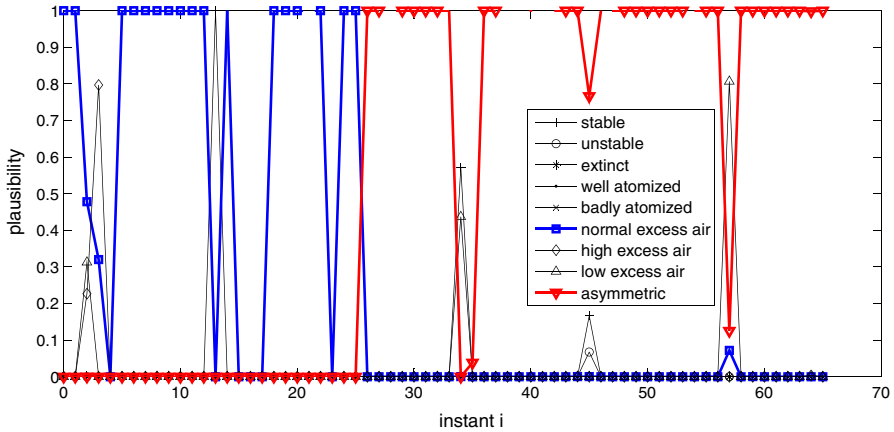

FIGURE 23 Plausibility functions for Test 4: Transition from normal excess air to asymmetric

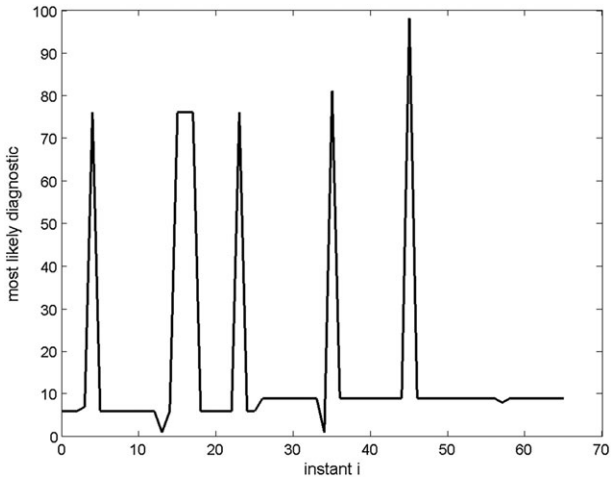

FIGURE 24 Most likely diagnostics for Test 4: Transition from normal excess air to asymmetric

7 | CONCLUSIONS

The present work has investigated the adequacy of the Dempster–Shafer method to mirror the ability of expert human operators to correlate flame visual patterns with distinct furnace operational states and to use such knowledge to issue reliable diagnostics on the combustion process status.

Through a suitable combination of five operational parameters, a test conducted at an experimental oil furnace equipped with an image-grabber system produced sets of flame images resulting from nine characteristic combustion states, classified by human experts as stable, unstable, extinct, well atomized, badly atomized, normal excess air, low excess air, high excess air, and asymmetric. Thereafter, computational processing created training and test feature vectors representing the salient visual characteristics of those sets.

Following the paradigm of the Dempster–Shafer method, a knowledge base was built by combining one to nine feature vectors in worlds that reflect the degree of confusion among multiple possible diagnostics. Next, an inference engine read a test feature vector, consulted the group of artificial experts, and using the Dempster–Shafer rule to combine the multiple individual diagnostics generated a comprehensive diagnosis expressing the degrees of belief and plausibility for all classes of flames.

Results indicated that the proposed inference engine could recognize most sudden changes in the combustion process resulting from the modification of real-world parameters, such as steam-to-fuel ratio, primary-to-secondary air flow ratio, and excess air. Still, in view of the tests performed, it might be argued that some diagnostics were not totally correct, which could represent a drawback of the method. Nevertheless, the incidence of those misclassification errors can be diminished either by including new correctly classified flame images in the training set or by introducing other, more discerning properties in the feature vectors. Additionally, it must be stressed that the errors reported by the diagnostic system, for most of the cases, were related to flames that, although belonging to distinct categories, did exhibit images with common features, which would be hard for a human expert to distinguish.

Thus, the above rationale suggests that such an approach might be used in the design of an automatic control system in industrial environments, with the advantages of a low cost and a simplicity of implementation. Moreover, if the images of flames used in the training and test sets are replaced by a new category of images concerning another domain of knowledge, the framework proposed in this article could be directly applied to generate proper diagnostics for that domain, provided convenient new features are adopted in order to enhance the most distinctive

aspects of those images. It must be emphasized, however, that all those tasks can only be accomplished once matters concerning real-time processing of data by the Dempster–Shafer inference engine are thoroughly investigated.

The design of automatic control strategies for oil refinery furnaces supported by a real-time Dempster–Shaper diagnosis expert system is part of the research currently under work by the authors of this paper.

ACKNOWLEDGEMENTS

The authors wish to thank the Conselho Nacional de Pesquisa e Desenvolvimento Tecnológico for supporting this work.

ORCID

A.T. Fleury http://orcid.org/0000-0002-0560-1556
F.C. Trigo http://orcid.org/0000-0002-0411-3243
A.L. Pacífico http://orcid.org/0000-0003-1355-1891
F.P.R. Martins http://orcid.org/0000-0003-1800-589X

REFERENCES

Basir, O., & Yuan, X. (2007). Engine-fault diagnosis based on multi-sensor information fusion using Dempster–Shafer evidence theory. *Information Fusion*, *8*, 379–386.

Benslama, M., Batatia, H., & Messai, A. (2016). Chapter 10. Tracking radar (using the Dempster–Shafer theory). In *Transitions from digital communications to quantum communications: Concepts and prospects*. London: ISTE Ltd & Hoboken: John Wiley & Sons.

Chakravarthy, S. S. S., Vohra, A. K., & Gill, B. S. (2000). Predictive emission monitors (PEMS) for NOx generation in process heaters. *Computers and Chemical Engineering*, *23*, 1649–1659.

Chen, Y. (2016). Industrial information integration—A literature review 2006–2015. *Journal of Industrial Information Integration*, *2*, 30–64.

Cho, W. S., Ro, S. D., Kim, S. W., Jang, W. H., & Shon, S. S. (1998). The process modelling and simulations for the fault diagnosis of rotary kiln incinerator process. *Journal of Industrial and Engineering Chemistry*, *4*, 99–104.

Fleury, A. T., Chui, D. S., Trigo, F. C., & Martins, F. P. R.(2015). Modeling, identification and a first control approach on the quality of flames in oil furnaces. In The 8th International Conference on Integrated Modeling and Analysis in Applied Control and Automation (IMAACA 2015). September 21–23, Bergeggi, Italy, pp. 79–88.

Fleury, A. T., Trigo, F. C., & Martins, F. P. R. (2013). A new approach based on computer vision and non-linear Kalman filtering to monitor the nebulization quality of oil flames. *Expert Systems with Applications*, *4*, 4760–4769.

Gonzalez, R. C., & Woods, R. E. (2008). *Digital image processing* (3rd ed.). New York: Prentice-Hall.

Hernández, R., & Ballester, J. (2008). Flame imaging as a diagnostic tool for industrial combustion. *Combustion and Flame*, *155*, 509–528.

Hughes, G. R., & Cresswell, M. J. (1972). *An introduction to modal logic*. London: Methuen and Co. Ltd.

Jamrozik, W. (2015). Contextual reliability discounting in welding process diagnostics based on DSmT. *Expert Systems*, *32*(2), 192–202.

Kessentini, Y., Burger, T., & Paquet, T. (2015). A Dempster–Shafer theory based combination of handwriting recognition systems with multiple rejection strategies. *Pattern Recognition*, *48*, 534–544.

Lefebvre, A. H. (1989). *Atomization and sprays*. Boca Raton: Taylor & Francis.

Li, W., & Chang, X. (2000). Application of hybrid fuzzy logic proportional plus conventional integral-derivative controller to combustion control of stocker–fired boilers. *Fuzzy Sets and Systems*, *111*, 267–284.

Malamas, E. N., Petrakis, E. G. M., Zervakis, M., Petit, L., & Legat, J. D. (2003). A survey on industrial vision systems, applications and tools. *Image and Vision Computing*, *21*, 171–188.

Murphy, R. R. (1998). Dempster–Shafer theory for sensor fusion in autonomous robots. *IEEE Transactions on Robotics and Automation*, *14*, 197–206.

Otsu, N. (1979). A threshold selection method from gray-level histograms. *IEEE Transactions on Systems, Man, and Cybernetics*, *9*, 62–66.

Pande, D., Sondawale, M., Keswani, G., & Walke, P. (2015). Dempster–Shafer theory based uncertainty quantification in air traffic management. *International Journal of Innovative Research in Science, Engineering and Technology*, *4*(12), 11886–11893.

Pandit, V. R., & Bhiwani, R. J. (2015). Image fusion in remote sensing applications: A review. *International Journal of Computer Applications*, *120*(10), 22–32.

Ranjidha, A., Kumar, A. R., & Saranya, M. (2013). Survey on medical image retrieval based on shape features and relevance vector machine classification. *International Journal of Emerging Trends and Technology in Computer Science*, *2*(3), 333–339.

Santos-Victor, J. A., Costeira, J. P., Tomé, J. A. B., & Sentieiro, J. J. S. (1993). A computer vision system for the characterization and classification of flames in gas furnaces. *IEEE Transactions on Industry Applications*, *29*(3), 470–478.

Sentz, K., & Ferson, S.(2002). Combination of evidence in Dempster–Shafer theory. Technical Report SAND 2002–0835.

Silva, R. P., Fleury, A. T., Martins, F. P. R., & Ponge-Ferreira, W. J. A. (2015). Identification of the state-space dynamics of oil flames through computer vision and modal techniques. *Expert Systems with Applications*, *42*, 2421–2428.

Tronci, S., Baratty, R., & Servida, A. (2002). Monitoring pollutant emissions in a 4.8 MW power plant through neural network. *Neurocomputing*, *43*, 3–15.

Turns, S. R. (2012). *An introduction to combustion: Concepts and applications* (3rd ed.). New York: McGraw-Hill.

Yan, Y., Lu, G., & Colechin, M. (2002). Monitoring and characterization of pulverised coal flames using digital imaging techniques. *Fuel*, *81*, 647–656.

Zadeh, L. (1986). A simple view of the Dempster–Shafer theory of evidence and its implication for the rule of combination. *Thennn*, *7*, 85–90.

Agenor de Toledo Fleury earned a degree in Mechanical Engineering from ITA/Aeronautics Technological Institute (1973) and MSc (1978) and PhD degrees in Mechanical Engineering from Escola Politecnica, University of São Paulo (1985). He is currently a professor at Escola Politecnica. He has led various projects at INPE, Brazilian Institute of Space Research, at Embraer, Brazilian Aeronautic Company, and at IPT, Sao Paulo State Institute for Technological Research, and at FEI University, most with emphasis on Dynamics and Control Systems. His most recent projects address modelling and control of nonlinear systems, optimal control, and estimation, in applications of Biomechanics, Robotics, Clean Combustion, and Automotive Engineering.

Flávio Celso Trigo graduated in Mechanical Engineering (1985) and received a PhD in Mechanical Engineering at Escola Politecnica, University of São Paulo (2005). Since 2008, he works as a professor/researcher at the Department of Mechanical Engineering of Escola Politecnica, Polytechnic School - University of São Paulo, Brazil. His main research interests include real-time parameter estimation and system identification through nonlinear techniques and its applications to biological and industrial impedance tomography, flame dynamics modelling and controlling, modelling and simulation of multibody systems, and sensor fusion for inertial guidance.

Antonio Luis Pacífico graduated in Mechanical Engineering (1990) at State University of Campinas, received the MSc (1995) and the PhD degrees (2000) in Mechanical Engineering at Escola Politecnica, University of São Paulo. He is a professor at the Department of Mechanical Engineering of Escola Politecnica, University of São Paulo and full professor at Maua Institute of Technology (Brazil). His major areas of research are flow measurement techniques, fluid–structure interaction, applications of low speed aerodynamics, atomization and sprays, optimization of thermo-fluid systems, and combustion measurement techniques.

Flavius Portella Ribas Martins graduated (1979) and received a MSc (1981) in Naval Engineering from Escola Politecnica, University of São Paulo (1979). In 1999, he received a PhD in Mechanical Engineering from Escola Politecnica, University of Sao Paulo. Since 2008, he works as professor/researcher at the Department of Mechanical Engineering, University of São Paulo. His current research interests include artificial intelligence, computer vision, and theoretical mechanics.

How to cite this article: Fleury AT, Trigo FC, Pacífico AL, Martins FPR. An inference model for combustion diagnostics in an experimental oil furnace. *Expert Systems*. 2018;35:e12245. https://doi.org/10.1111/exsy.12245